Orbital structure and magnetic ordering in layered manganites: Universal correlation and its mechanism

S. Okamoto, S. Ishihara, and S. Maekawa
Institute for Materials Research, Tohoku University, Sendai 980-8577, Japan
(Received 14 June 2000; revised manuscript received 5 September 2000; published 6 February 2001)

Correlation between orbital structure and magnetic ordering in layered manganites is examined. A level separation between the $3d_{3z^2-r^2}$ and $3d_{x^2-y^2}$ orbitals in a Mn ion is calculated in the ionic model for a large number of the compounds. It is found that the relative stability of the orbitals dominates the magnetic transition temperatures as well as the magnetic structures at zero temperature. A mechanism of the correlation between orbital and magnetism is explained by a theory based on the model with the two e_g orbitals under strong electron correlation.

DOI: 10.1103/PhysRevB.63.104401 PACS number(s): 75.30.Vn, 71.10.−w, 75.30.Kz, 75.80.+q

Since the discovery of the colossal magnetoresistance (CMR), studies of manganites with pseudocubic structure have been renewed theoretically and experimentally. Competition and cooperation between spin, charge, and orbital degrees of freedom as well as lattice cause the dramatic changes of transport and magnetic properties. Manganites with layered crystal structure $A_{2-2x}B_{1+2x}Mn_2O_7$, where A and B are trivalent and divalent cations, respectively, are another class of CMR materials.[1,2] One of the consequence of reduced dimensionality in these compounds is the strong anisotropy in the electrical resistivity and the magnetic structures as well as the large magnitude of CMR near the transition from paramagnetic (PM) insulator to ferromagnetic (FM) metal.

In pseudocubic manganites, competition between itinerant ferromagnetism and carrier localization accompanied by the antiferromagnetism (AFM) dominates its unique magnetotransport. The correlations between magnetic orderings and several structural parameters have been investigated. It is shown that the magnetic transition temperature is systematically varied as a function of the average ionic radius $\langle r_A \rangle$ of cations at the perovskite A site which is supposed to control magnitudes of the hopping integral for carriers.[3,4] It has been considered that several concepts proposed in the pseudocubic manganites are applicable to the layered ones where a variety of magnetic structures are also observed. Various key factors dominating the magnetic ordering were experimentally suggested, e.g., the AFM superexchange (SE) interaction,[5] the local lattice distortion,[6–9] the charge and orbital degrees of freedom and their orderings[10,11] and so on. However, systematics in their correlations for a variety of compounds and their mechanisms still remain to be clarified.

In this paper, we study the correlation between magnetic ordering and orbital structure in layered manganites. The two e_g orbitals, i.e., the $3d_{3z^2-r^2}$ and $3d_{x^2-y^2}$ orbitals in a Mn^{3+} ion split in the crystalline field of the layered crystal structure and one of them is occupied by an electron. It is known that the occupied orbital controls the anisotropy of the magnetic interaction as well as its strength. The level separation between the orbitals is calculated in the ionic model for a large number of the compounds. We find a universal correlation between the relative stability of the orbitals and the magnetic transition temperatures as well as the magnetic structures. A mechanism of the correlation is explained by a theory based on the model with the e_g orbitals under strong electron correlation.

We first show that in layered manganites neither the tolerance factor which reflects $\langle r_A \rangle$ nor the bond length governs T_C and the Néel temperature T_N for the A-type AFM ordering. In layered manganites, the following two layered AFM structures have been observed: [12,13] AFM-I consisting of the FM spin ordering in the plane and the AFM (FM) one along the c axis within [between nearest-neighboring (NN)] bilayers, and AFM-II consisting of the FM in the plane and the FM (AFM) along the c axis within (between NN) bilayers. Since the intrabilayer magnetic coupling is much larger than the interbilayer one,[14] we term the AFM-I structure the A-type AFM one and regard the AFM-II as the FM. The tolerance factor in the bilayered crystal structure is defined by $t=(t_1+t_2)/2$ with

$$t_l=\frac{d_{\mathrm{O}(l)-A(l)}}{\sqrt{2}d_{\mathrm{Mn\text{-}O(3)}}}, \tag{1}$$

where $d_{\mathrm{A\text{-}B}}$ is a bond length between A and B ions. The position of each ion is shown in the inset of Fig. 1(a). Being

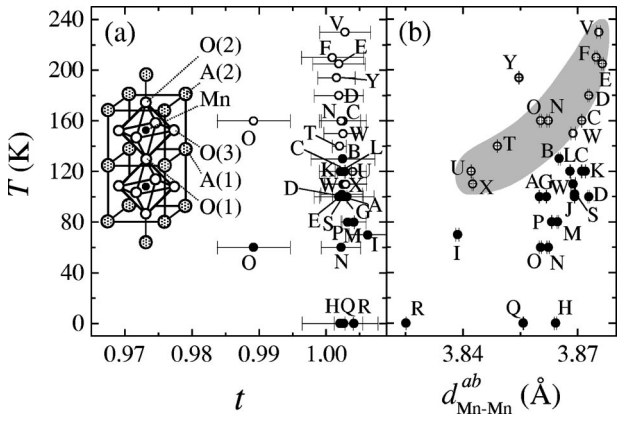

FIG. 1. T_C and T_N as functions of (a) t and (b) $d^{ab}_{\mathrm{Mn\text{-}Mn}}$. Filled and open circles indicate T_C and T_N, respectively. t and $d^{ab}_{\mathrm{Mn\text{-}Mn}}$ are obtained from the structural data in the compounds listed in Table I. The inset of (a) shows a schematic picture of the bilayered structure.

TABLE I. The structural data of bilayered manganites used in the present examination. Listed are the labels, the chemical formulas, the Curie temperatures for FM ordering, the Néel temperatures for A-type AFM ordering, references for the structure and magnetic data, and types of the samples, where *s* and *p* indicate a single crystal and a polycrystal, respectively. The labels in the first column are used in Figs. 1–3.

Symbol	sample	T_C(K)	T_N(K)	Ref.	*s*/*p*
A	$La_{1.4}Sr_{1.6}Mn_2O_7$	100	–	12	*s*
B	$La_{1.3}Sr_{1.7}Mn_2O_7$	130	–	12	*p*
C	$La_{1.2}Sr_{1.8}Mn_2O_7$	120	160	12	*s*
D	$La_{1.1}Sr_{1.9}Mn_2O_7$	100	180	12	*s*
E	$La_{1.04}Sr_{1.96}Mn_2O_7$	0	205	12	*s*
F	$LaSr_2Mn_2O_7$	–	210	12	*s*
G	$La_{1.4}Sr_{1.6}Mn_2O_7$	100	–	13	*p*
H	$Pr_{1.4}Ca_{1.3}Ba_0.3Mn_2O_7$	0	–	15	*p*
I	$Nd_{1.4}Ca_{1.6}Mn_2O_7$	70	–	15	*p*
J	$La_{1.4}Sr_{1.6}Mn_2O_7$	100	–	16	*p*
K	$La_{1.2}Sr_{1.8}Mn_2O_7$	120	–	17	*p*
L	$La_{1.2}Sr_{1.8}Mn_2O_7$	120	–	18	*s*
M	$La_{1.2}(Sr_{0.8}Ca_{0.2})_{1.8}Mn_2O_7$	80	–	18	*s*
N	$La_{1.2}(Sr_{0.7}Ca_{0.3})_{1.8}Mn_2O_7$	60	160	18	*s*
O	$La_{1.2}(Sr_{0.6}Ca_{0.4})_{1.8}Mn_2O_7$	60	160	18	*p*
P	$(La_{0.8}Nd_{0.2})_{1.2}Sr_{1.8}Mn_2O_7$	80	–	18	*s*
Q	$(La_{0.6}\|Nd_{0.4})_{1.2}Sr_{1.8}Mn_2O_7$	0	–	18	*s*
R	$Sm_{1.2}Sr_{1.8}Mn_2O_7$	0	–	19	*p*
S	$La_{1.2}Sr_{1.4}Ca_{0.4}Mn_2O_7$	100	–	20	*p*
T	$NdSr_2Mn_2O_7$	–	140	21	*p*
U	$Nd_{1.1}Sr_{1.9}Mn_2O_7$	–	120	21	*p*
V	$LaSr_2Mn_2O_7$	–	230	22	*p*
W	$LaSr_{1.6}Ca_{0.4}Mn_2O_7$	110	150	23	*p*
X	$NdSr_2Mn_2O_7$	–	110	23	*s*
Y	$La_{0.84}Sr_{2.16}Mn_2O_7$	–	194	24	*p*

based on the structural data obtained by the neutron and x-ray diffraction experiments listed in Table I, [12,13,15–24] we evaluate t and the bond length between NN Mn ions in the ab plane $d^{ab}_{\text{Mn-Mn}}$ for a variety of compounds. For the samples *G*, *J*, *R*, *T*, and *U* where the two chemically distinct phases are observed, the structural data of the major phase are adopted. T_C and T_N are plotted as functions of t and $d^{ab}_{\text{Mn-Mn}}$ in Figs. 1(a) and 1(b), respectively. Almost all t's are located in a narrow region where T_C's and T_N's are distributed randomly. We also examine the correlations between $T_{C(N)}$ and the each term of t, i.e., t_l for $l=1$ and 2. The results are similar to that in Fig. 1(a). In addition, T_C is not correlated with $d^{ab}_{\text{Mn-Mn}}$, either. Although T_N increases with increasing $d^{ab}_{\text{Mn-Mn}}$, this correlation is opposite to that predicted by the conventional double-exchange (DE) scenario where, with increasing the bond length, the hopping integral decreases and the FM interaction in the ab plane decreases. We conclude that the DE model, which includes the change of the hopping integral caused by the change of the bond angle/length, cannot explain $T_{C(N)}$. We also examined correlations between $T_{C(N)}$ and a number of other quantities: the tolerance factor evaluated by the ionic radius, a Mn-O(3)-Mn bond angle, a Mn-O(1)-Mn bond length, Mn-O bond lengths, a lattice spacing between NN bilayers, lattice constants, the valence-bond sum for a Mn ion, and the cation size disorder.[25] However, there are not clear correlations between these parameters and $T_{C(N)}$.

Let us focus on the correlation between $T_{C(N)}$ and a relative stability of the e_g orbitals. We employ the ionic model to examine the electronic energy-level structures. This model may be justified for the energy-level structures for Mn $3d$ e_g orbitals of the present interest by the following considerations:[26] (1) the manganites at $x=0$ are ionic insulators, and the ionic model provides a good starting point in this class of materials.[27,28] (2) The ionic property is predominant between bilayers. (3) The energy-level structure given by calculations where the covalency effects between Mn $3d$ and O $2p$ orbitals are taken into account shows the same tendency with those by the ionic model.[7,29] This is because, in this energy-level structure, one electron occupies one of the two antibonding orbitals with lower energy resulted from the mixing between the Mn e_g orbitals and the O $2p$ ones in NN O ions. The covalency effects between Mn $3d$ orbitals in different Mn ions will be considered later. The energy levels of the e_g orbitals split due to the electrostatic potential and one of the orbitals is occupied by an electron in a Mn^{3+} ion. By using a large number of the structural data,[12,13,15–24] we calculate the Madelung potential for a hole in the $3d_{3z^2-r^2}$ and $3d_{x^2-y^2}$ orbitals at site j defined by

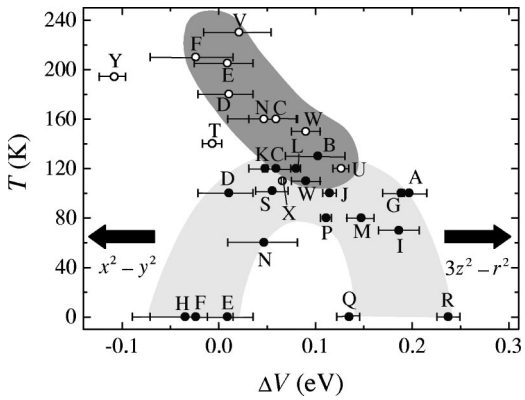

FIG. 2. T_C and T_N as functions of ΔV. Filled and open circles indicate T_C and T_N, respectively. ΔV's are calculated for the same compounds in Fig. 1. Note that in the region with large positive (negative) ΔV, the $3d_{3z^2-r^2}$ ($3d_{x^2-y^2}$) orbital is occupied by an electron.

$$V_{3z^2-r^2}=\frac{1}{2}\{V(\vec{r}_j+r_d\hat{z})+V(\vec{r}_j-r_d\hat{z})\}, \tag{2}$$

and

$$V_{x^2-y^2}=V(\vec{r}_j+r_d\hat{x}), \tag{3}$$

respectively.[30] Here, $V(\vec{r}_j)$ is given by

$$V(\vec{r}_j)=\sum_{i\neq j}\frac{Z_i e^2}{|\vec{r}_j-\vec{r}_i|}, \tag{4}$$

with a point charge $Z_i e$ at site i and the position $\vec{r}_i$ of the site. $r_d(=0.42\text{Å})$ is the radius of a Mn $3d$ orbital where its radial charge density becomes maximum[31] and $\hat{z}(\hat{x})$ is the unit vector in the $z(x)$ axis. The Ewald method is used for the lattice summation. Z_i's for Mn and O ions and a cation at A site are chosen to be $3+x$, -2, and $(8-2x)/3$, respectively. The difference of the potentials

$$\Delta V=V_{3z^2-r^2}-V_{x^2-y^2}, \tag{5}$$

represents the relative stability of the orbitals; with increasing ΔV, the energy level of the $3d_{3z^2-r^2}$ orbital for an electron relatively decreases.

T_N and T_C are plotted as functions of ΔV in Fig. 2 where the structural data at room temperature are used. Broad shades are drawn by considering experimental errors. It is clearly shown that both T_C and T_N are correlated with ΔV; T_N increases with decreasing ΔV and there is an optimal value of $\Delta V(\sim 0.08$ eV) for T_C. We estimate the strength of the correlation between T_N and ΔV by using the correlation coefficient:

$$r=\frac{1}{N}\sum_l\frac{(T_{Nl}-\overline{T_N})(\Delta V_l-\overline{\Delta V})}{\sigma_{T_N}\sigma_{\Delta V}}, \tag{6}$$

where l indicates a sample and N is the number of samples. $\overline{\Delta V}$ ($\overline{T_N}$) and $\sigma_{\Delta V}$ (σ_{T_N}) are the mean value and the standard deviation of ΔV (T_N), respectively. We obtain $r=-0.89\pm 0.12$ for single crystal samples and $r=-0.19\pm 0.05$ for all samples including polycrystals. One might think that the $T_{C(N)}$ vs ΔV curve in Fig. 2 just reflects the relation between $T_{C(N)}$ and x in $La_{2-2x}Sr_{1+2x}Mn_2O_7$ (LSMO).[12,8] However, when we pay attention to $T_{C(N)}$'s for samples with the same x (e.g., the samples C and K-R), we notice that the correlation remains. The correlation between T_N and ΔV explains that between T_N and $d^{ab}_{\text{Mn-Mn}}$ shown in Fig. 1(b), since ΔV is a decreasing function of $d^{ab}_{\text{Mn-Mn}}$ in the region, 3.84 Å $<d^{ab}_{\text{Mn-Mn}}<3.88$ Å.

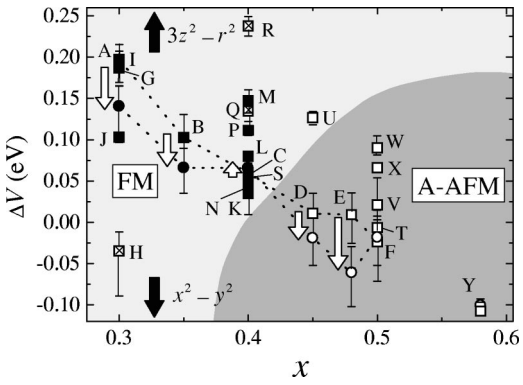

FIG. 3. The magnetic phase diagram at $T=0$ as a function of ΔV and x. Filled, open, and crossed squares indicate the FM, A-type AFM and PM samples, respectively. ΔV's for filled and open circles are obtained from the data below T_C and T_N, respectively. Symbols connected by dotted lines indicate a series of LSMO. Bold arrows show $\delta(\Delta V)=\Delta V(T<T_{C(N)})-\Delta V(T>T_{C(N)})$. ΔV's are calculated for the same compounds in Fig. 1. Note that in the region with large positive (negative) ΔV, the $3d_{3z^2-r^2}$ ($3d_{x^2-y^2}$) orbital is occupied by an electron.

In Fig. 3, we present the magnetic phase diagram at $T=0$ as a function of ΔV and x. The structural data at room temperature are used. Symbols connected by dotted lines correspond to a series of LSMO with $x=0.3\sim 0.5$.[12] In addition, ΔV's calculated by using the data below $T_{C(N)}$ in LSMO are also plotted. Bold arrows indicate the change of the Madelung potential with changing temperature from $T>T_{C(N)}$ to $T<T_{C(N)}$:

$$\delta(\Delta V)\equiv\Delta V(T<T_{C(N)})-\Delta V(T>T_{C(N)}). \tag{7}$$

We find that the magnetic structures are governed by ΔV and x; the FM (A-type AFM) phase is located in the region with smaller (larger) x and moderate (smaller) ΔV. Let us focus on $\delta(\Delta V)$ in LSMO. $\delta(\Delta V)$'s are negative at $x=0.3$ and 0.35. The absolute value of $\delta(\Delta V)$ gradually decreases with increasing x and $\delta(\Delta V)$ becomes a small positive value at $x=0.4$. Below T_C, ΔV seems to approach to the optimal value of $\Delta V\sim 0.08$ where T_C becomes maximum as seen in Fig. 2. On the other hand, $\delta(\Delta V)$'s are negative at $x=0.45$ and 0.48 where the A-type AFM structure appears. The orbital structure and its stability in the FM phase have been studied by measuring the striction in Ref. 11. The difference of the Mn-O bond lengths between PM and FM states was reported in Ref. 8. These experimental results are consistent with the present results of $\delta(\Delta V)$ in Fig. 3.

Now we theoretically investigate a mechanism of the correlation between magnetic ordering and orbital structure. Instead of the bilayered structure, the simple tetragonal lattice consisting of Mn ions is considered. In this model, the magnetic structure with FM and AFM alignments perpendicular and parallel to the c axis, respectively, corresponds to the A-type AFM structure. In each Mn ion, the two e_g orbitals are introduced and the t_{2g} electrons are treated as a localized spin. We start with the following tight-binding Hamiltonian:

$$\mathcal{H}=\mathcal{H}_{e_g}+\mathcal{H}_{AF}+\mathcal{H}_H. \tag{8}$$

The first term describes electrons in the e_g orbitals and is given by

$$\mathcal{H}_{e_g}=\sum_{i\gamma\sigma}\varepsilon_\gamma d^\dagger_{i\gamma\sigma}d_{i\gamma\sigma}+\sum_{\langle ij\rangle\gamma\gamma'\sigma}t_{ij}^{\gamma\gamma'}(d^\dagger_{i\gamma\sigma}d_{j\gamma'\sigma}+H.c.)$$
$$+U\sum_{i\gamma}n_{i\gamma\uparrow}n_{i\gamma\downarrow}+U'\sum_{i\sigma\sigma'}n_{ia\sigma}n_{ib\sigma'}$$
$$+I\sum_{i\sigma\sigma'}d^\dagger_{ia\sigma}d^\dagger_{ib\sigma'}d_{ia\sigma'}d_{ib\sigma}, \tag{9}$$

where $d_{i\gamma\sigma}$ is an annihilation operator of the e_g electron at site i with spin σ and orbital γ and $n_{i\gamma\sigma}=d^\dagger_{i\gamma\sigma}d_{i\gamma\sigma}$ is the number operator. The splitting between the energy levels of $3d_{3z^2-r^2}$ and $3d_{x^2-y^2}$ orbitals is represented by Δ as $\varepsilon_{x^2-y^2}-\varepsilon_{3z^2-r^2}=\Delta$. The second term describes the electron hopping between NN Mn sites where the orbital dependence of $t_{ij}^{\gamma\gamma'}$ is determined by the Slater-Koster formulas.[31] The last three terms represent the Coulomb interactions between e_g electrons where U, U', and I are the intra-orbital Coulomb interaction, the interorbital one and the exchange interaction, respectively. The second and third terms in Eq. (8) are given by

$$\mathcal{H}_H+\mathcal{H}_{AF}=-J_H\sum_i\vec{S}_i\cdot\vec{S}_{t_{2g}i}+\sum_{\langle ij\rangle}J^l_{AF}\vec{S}_{t_{2g}i}\cdot\vec{S}_{t_{2g}j}, \tag{10}$$

where $\vec{S}_i$ and $\vec{S}_{t_{2g}i}$ are spin operators for the e_g and t_{2g} electrons with $S=1/2$ and 3/2, respectively, J_H is the Hund coupling between e_g and t_{2g} spins and J^l_{AF} is the AFM SE interaction between the NN t_{2g} spins in $l(=x,y,z)$ direction. Since the Coulomb interactions between e_g electrons provide the largest energy parameter, we derive the effective Hamiltonian describing the electronic states in low energy regions by the perturbational calculation with respect to (the hopping integral)/(the Coulomb interactions) as follows

$$\tilde{\mathcal{H}}=\mathcal{H}_t+\mathcal{H}_J+\mathcal{H}_\Delta+\mathcal{H}_H+\mathcal{H}_{AF}. \tag{11}$$

The first and second terms in Eq. (11) correspond to the so-called t and J terms in the tJ model:

$$\mathcal{H}_t=\sum_{\langle ij\rangle\gamma\gamma'\sigma}t_{ij}^{\gamma\gamma'}\tilde{d}^\dagger_{i\gamma\sigma}\tilde{d}_{j\gamma'\sigma}+H.c., \tag{12}$$

and

$$\mathcal{H}_J=-2\sum_{\langle ij\rangle}J^l_1\left(\frac{3}{4}n_in_j+\vec{S}_i\cdot\vec{S}_j\right)\left(\frac{1}{4}-\tau^l_i\tau^l_j\right)$$
$$-2\sum_{\langle ij\rangle}J^l_2\left(\frac{1}{4}n_in_j-\vec{S}_i\cdot\vec{S}_j\right)\left(\frac{3}{4}+\tau^l_i\tau^l_j+\tau^l_i+\tau^l_j\right)+\mathcal{H}^\Delta_J, \tag{13}$$

where $\tau^l_i=\cos[(2\pi/3)m_l]T_{iz}-\sin[(2\pi/3)m_l]T_{ix}$ with $(m_x,m_y,m_z)=(1,2,3)$, and l denotes a direction of the bond connecting site i and site j. $\tilde{d}_{i\gamma\sigma}$ is the annihilation operator of the e_g electron with excluding double occupancy of electron and n_i is the number operator defined as $n_i=\Sigma_{\gamma\sigma}\tilde{d}^\dagger_{i\gamma\sigma}\tilde{d}_{i\gamma\sigma}$. $\vec{T}_i$ is the pseudospin operator for the orbital degree of freedom defined as $\vec{T}_i=(1/2)\Sigma_{\gamma\gamma'\sigma}\tilde{d}^\dagger_{i\gamma\sigma}(\vec{\sigma})_{\gamma\gamma'}\tilde{d}_{i\gamma'\sigma}$, where $T_{iz}=+(-)1/2$ corresponds to the state where the $d_{3z^2-r^2}$ ($d_{x^2-y^2}$) orbital is occupied by an electron. J^l_1 and J^l_2 are defined by $J^l_1=t_0^{l2}/(U'-I)$ and $J^l_2=t_0^{l2}/(U+2J_H)$ where t^l_0 is the hopping integral between NN $d_{3l^2-r^2}$ orbitals in l direction. $\mathcal{H}^\Delta_J$ in Eq. (13) is a correction of the J term being of the order of Δ/U given by

$$\mathcal{H}^\Delta_J=-\frac{\Delta}{2}\sum_{\langle ij\rangle}\frac{1}{t_0^{l2}}\left\{J_1^{l2}\left(\frac{3}{4}n_in_j+\vec{S}_i\cdot\vec{S}_j\right)+J_2^{l2}\left(\frac{1}{4}n_in_j\right.\right.$$
$$\left.\left.-\vec{S}_i\cdot\vec{S}_j\right)\right\}\sin\left(\frac{2\pi}{3}m_l\right)(o^l_in_j+n_io^l_j), \tag{14}$$

with $o^l_i=\sin[(2\pi/3)m_l]T_{iz}+\cos[(2\pi/3)m_l]T_{ix}$. The splitting of the energy levels between $3d_{3z^2-r^2}$ and $3d_{x^2-y^2}$ orbitals is represented by $\mathcal{H}_\Delta$ defined as

$$\mathcal{H}_\Delta=-\Delta\sum_i T_{iz}. \tag{15}$$

The anisotropies of the hopping integral and the SE interactions due to the layered structure are considered as $t^x_0=t^y_0\equiv t_0$ and $J^x_{AF}=J^y_{AF}$ with the parameter $R=t^x_0/t^z_0=\sqrt{J^x_1/J^z_1}=\sqrt{J^x_2/J^z_2}=\sqrt{J^x_{AF}/J^z_{AF}}$. When we assume $\Delta=0$ and $R=1$, $\tilde{\mathcal{H}}$ is reduced to the effective Hamiltonian for pseudo-cubic manganites derived in Ref. 32.

The magnetic phase diagram is calculated by the mean-field approximation. We consider four types of the spin and orbital ordered states; ferromagnetic(F)-type state where spin and orbital states are uniform, and layer (A)-type, rod (C)-type, and NaCl(G)-type antiferromagnetic states where the two kinds of spin and orbital sublattices exist. $\langle S_z\rangle$, $\langle T_z\rangle$, $\langle T_x\rangle$ and $\langle n\rangle$ are adopted as order parameters. $\langle S_z\rangle=\frac{1}{3}\langle S_{t_{2g}z}\rangle$ is assumed because of the strong Hund coupling. In $\mathcal{H}_t$, the rotating frames in both the spin and orbital spaces are introduced and the electron annihilation operator is represented by using the unitary matrices of the rotations as $\tilde{d}_{i\gamma\sigma}=h^\dagger_i z^s_\sigma z^t_\gamma$ where $h^\dagger_i$ is the creation operator of a spin- and orbital-less fermion, and $z^{s(t)}_{i\sigma(\gamma)}$ is an element of the unitary matrix in the spin(orbital) frame. These are given by $z^s_{i\uparrow}=\cos(\theta^s_i/2)e^{-i\phi^s_i/2}$, $z^s_{i\downarrow}=\sin(\theta^s_i/2)e^{i\phi^s_i/2}$, $z^t_{ia}=\cos(\theta^t_i/2)$,

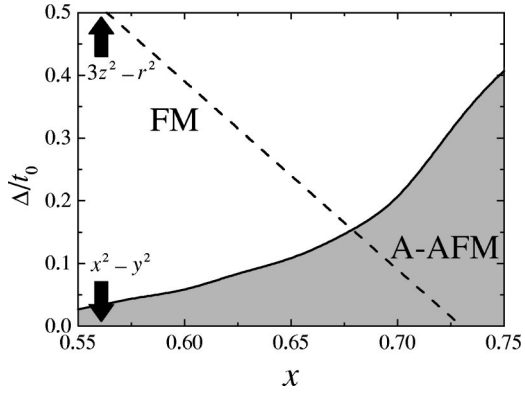

FIG. 4. The calculated magnetic phase diagram at $T=0$ as a function of Δ and x. Note that in the region with large positive (negative) Δ, the $3d_{3z^2-r^2}$ ($3d_{x^2-y^2}$) orbital is occupied by an electron. The broken line indicates the parameter values of Δ and x adopted in the calculation for Fig. 5.

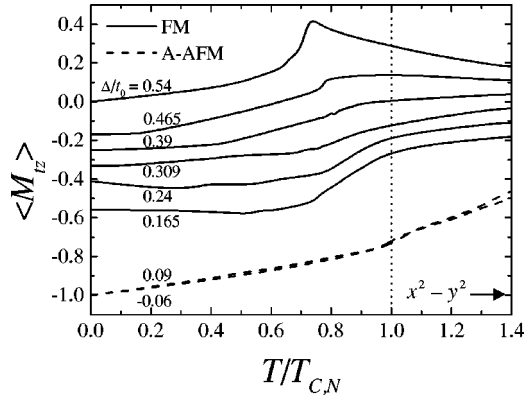

FIG. 5. The temperature dependence of the orbital order parameter $\langle M_{tz}\rangle$ for several values of Δ. The parameter values are the same with those adopted in Fig. 4. A value of Δ together with x is changed along the broken line in Fig. 4. The solid and broken lines show $\langle M_{tz}\rangle$'s in the cases where the FM and *A*-type AFM orderings are realized at $T=0$, respectively.

and $z^t_{ib}=\sin(\theta^t_i/2)$. Here, the polar angle $\theta^{s(t)}_i$ and the azimuthal angle ϕ^s_i are determined by types of the spin (orbital) ordered states in the mean fields. The detailed formulation of this approximation is presented in Ref. 33. We note that the phase diagram for pseudocubic manganites derived in this approximation explains the several experimental results and are consistent with the theoretical results obtained by other approximations.[34] The phase diagram at $T=0$ for the manganites with bilayered structure has also been studied in the Hartree-Fock theory in Ref. 35.

The calculated magnetic phase diagram at $T=0$ is presented in Fig. 4. The parameter values are chosen to be $J^x_1/t^x_0=0.25$, $J^x_2/t^x_0=0.075$, $J^x_{AF}/t^x_0=0.002$ and $R=1.5$. These values are determined from the experimental results of photoemission in pseudocubic manganites and the Néel temperature in $CaMnO_3$. In order to check the calculation, we compare the present results with the magnetic phase diagrams obtained by the following two calculations; (1) We adopt the model where a pair of two MnO_2 sheets is considered and the two sheets are coupled by the electron hopping and the SE interaction, instead of the simple tetragonal lattice, and (2) the mean-field approximation in the slave boson scheme is applied to the Hamiltonian in Eq. (11). The obtained phase diagrams are similar to that in Fig. 4. The characteristic features shown in Fig. 3 are well reproduced by the present theory; the *A*-type AFM phase appears in the region with higher x and smaller Δ than that of the FM one. The range of the horizontal axis in Fig. 4 is larger than that in Fig. 3 by about 0.25. This discrepancy may be attributed to the neglect of the orbital fluctuation.[36] However, the characteristics of the phase diagram are insensitive to the parameters in the model. In the FM (*A*-type AFM) phase, the orbitals are uniformly aligned with $0<\theta<0.72\pi$ ($0.72\pi<\theta<\pi$) where θ describes the orbital state as $|\theta\rangle=\cos(\theta/2)|3d_{3z^2-r^2}\rangle-\sin(\theta/2)|3d_{x^2-y^2}\rangle$. The present results suggest that a dimensionality of the FM interaction is controlled by the orbital structure; in the *A*-type AFM phase, the FM ordering in the ab plane is caused by the DE interaction, while the AFM in the c direction is by the AFM SE. When the $3d_{x^2-y^2}$ orbital is stabilized, the DE interaction in the ab plane (c direction) becomes strong (weak) and the *A*-type AFM phase appears.[37] A mixing of the orbitals is essential in the FM phase where the FM interaction overcomes the AFM SE one in the three directions. We note that, in Fig. 4, the FM phase appears not around $\Delta=0$ but in a region of $\Delta>0$, since the anisotropy in the hopping integral due to the layered structure stabilizes the $3d_{x^2-y^2}$ orbital more than $3d_{3z^2-r^2}$. It is worth mentioning the change of the orbital structure associated with the magnetic ordering: By utilizing the mean-field approximation at finite temperature, we examine change of the orbital structures through the magnetic transitions. In Fig. 5, we present the temperature dependence of the z component of the orbital order parameter defined by $\langle M_{tz}\rangle=\langle T_z\rangle/\langle\vec{T}^2\rangle_0^{1/2}$ where $\langle\cdots\rangle$ and $\langle\cdots\rangle_0$ indicate the thermal average and the average at $T=0$, respectively. $\langle M_{tz}\rangle=1$ and -1 correspond to the orbital ordered states where the $3d_{3z^2-r^2}$ and $3d_{x^2-y^2}$ orbitals are uniformly aligned, respectively. A value of Δ together with x is changed along the broken line in Fig. 4. It is found that (1) there is an optimal mixing of the orbitals for the FM state and the orbital structure tends to approach this structure below T_C, and (2) the $3d_{x^2-y^2}$ orbital structure is stabilized below T_N. The theoretical results are consistent with $\delta(\Delta V)$'s shown in Fig. 3 by considering that the change of ΔV associated with the magnetic ordering is caused by that of the orbital structure.

We note that the present mechanism of the correlation between orbital structure and magnetism also explains the *C*-type AFM phase recently observed in $La_{2-2x}Sr_{1+2x}Mn_2O_7$ with $0.74<x<0.92$.[24] In this phase, the ferromagnetic columns exist along b axis and the columns are antiferromagnetically coupled along a and c axes inside bilayers. Through the calculation of the Madelung potential based on the structural data,[24] we confirm that stability of the $3d_{3y^2-r^2}$ orbital increases in this magnetic phase. This is consistent with the theoretical results calculated from the model Eq. (11); the *C*-type AF phase associated with the uniform orbital ordered state of $3d_{3y^2-r^2}$ orbital appears in

the higher hole concentration region of the *A*-type AF phase. In this orbital ordered state, the FM ordering in the *b* direction is caused by the DE interaction, while the AFM SE interaction overcomes the DE one in the other two directions due to the $3d_{3y^2-r^2}$ orbital.

In summary, we examine correlation between magnetic ordering and orbital structure in layered manganites. A relative stability of the e_g orbitals is investigated by calculating the Madelung potentials in a large number of the compounds. We find that the *A*-type AFM structure and the $3d_{x^2-y^2}$ orbital one are stabilized cooperatively and there is an optimal mixing between the $3d_{3z^2-r^2}$ and $3d_{x^2-y^2}$ orbitals for the FM ordering. A theory with the two e_g orbitals under strong electron correlation explains a mechanism of the universal correlation between orbital and magnetism.

The authors would like to thank Y. Moritomo, T. Akimoto, Y. Tokura, T. Kimura, Y. Endoh, K. Hirota, M. Kubota, G. Khaliullin, and T. Hatakeyama for their valuable discussions. The authors also thank J. F. Mitchell for providing the experimental data prior to publication. This work was supported by CREST, NEDO, Grant-in-Aid for Scientific Research Priority Area from the Ministry of Education, Science and Culture of Japan, and Science and Technology Special Coordination Fund for promoting science and technology. S.O. acknowledges the financial support of JSPS. Part of the numerical calculation was performed in the HITACS-3800/380 supercomputing facilities in IMR, Tohoku University.

[1] Y. Moritomo, A. Asamitsu, H. Kuwahara, and Y. Tokura, Nature (London) **380**, 141 (1996).
[2] T. Kimura, Y. Tomioka, H. Kuwahara, A. Asamitsu, M. Tamura, and Y. Tokura, Science **274**, 1698 (1996).
[3] H. Y. Hwang, S.-W. Cheong, P. G. Radaeli, M. Marezio, and B. Batlogg, Phys. Rev. Lett. **75**, 914 (1995).
[4] S.-W. Cheong and H. Y. Hwang, in *Colossal Magnetoresisitance Oxides* edited by Y. Tokura (Gordon and Breach, Amsterdam, 2000).
[5] T. G. Perring, G. Aeppli, Y. Moritomo, and Y. Tokura, Phys. Rev. Lett. **78**, 3197 (1997).
[6] D. Louca, G. H. Kwei, and J. F. Mitchell, Phys. Rev. Lett. **80**, 3811 (1998).
[7] D. S. Dessau, T. Saitoh, C.-H. Park, Z.-X. Shen, P. Villella, N. Hamada, Y. Moritomo, and Y. Tokura, Phys. Rev. Lett. **81**, 192 (1998).
[8] M. Medarde, J. F. Mitchell, J. E. Millburn, S. Short, and J. D. Jorgensen, Phys. Rev. Lett. **83**, 1223 (1999).
[9] L. Vasiliu-Doloc, S. Rosenkranz, R. Osborn, S. K. Sinha, J. W. Lynn, J. Mesot, O. H. Seeck, G. Preosti, A. J. Fedro, and J. F. Mitchell, Phys. Rev. Lett. **83**, 4393 (1999).
[10] Y. Moritomo, Y. Maruyama, T. Akimoto, and A. Nakamura, Phys. Rev. B **56**, R7057 (1997).
[11] T. Kimura, Y. Tomioka, A. Asamitsu, and Y. Tokura, Phys. Rev. Lett. **81**, 5920 (1998).
[12] M. Kubota, H. Fujioka, K. Hirota, K. Ohoyama, Y. Moritomo, H. Yoshizawa, and Y. Endoh, J. Phys. Soc. Jpn. **69**, 1606 (2000).
[13] D. N. Argyriou, H. N. Bordallo, J. F. Mitchell, J. D. Jorgensen, and G. F. Strouse, Phys. Rev. B **59**, 8695 (1999).
[14] H. Fujioka, M. Kubota, K. Hirota, H. Yoshizawa, Y. Moritomo, and Y. Endoh, J. Phys. Chem. Solids **60**, 1165 (1999).
[15] P. Laffez, G. Van Tendeloo, R. Seshadri, M. Hervieu, C. Martin, A. Maignan, and B. Raveau, J. Appl. Phys. **80**, 5850 (1996).
[16] E.-O. Chi, K.-P. Hong, Y.-U. Kwon, N. P. Raju, J. E. Greedan, J.-S. Lee, and N. H. Hur, Phys. Rev. B **60**, 12 867 (1999).
[17] D. N. Argyriou, J. F. Mitchell, J. B. Goodenough, O. Chmaissem, S. Short, and J. D. Jorgensen, Phys. Rev. Lett. **78**, 1568 (1997).
[18] T. Akimoto, Y. Moritomo, K. Ohoyama, S. Okamoto, S. Ishihara, S. Maekawa, and A. Nakamura, Phys. Rev. B **59**, R14 153 (1999).
[19] P. D. Battle, N. Kasmir, J. E. Millburn, M. J. Rosseinsky, R. T. Patel, L. E. Spring, J. F. Vente, S. J. Blundell, W. Hayes, A. K. Klehe, A. Mihut, and J. Singleton, J. Appl. Phys. **83**, 6379 (1998).
[20] C. H. Shen, R. S. Liu, S. F. Hu, J. G. Lin, C. Y. Huang, and H. S. Sheu, J. Appl. Phys. **86**, 2178 (1999).
[21] P. D. Battle, M. A. Green, N. S. Laskey, J. E. Millburn, P. G. Radaelli, M. J. Rosseinsky, S. P. Sullivan, and J. F. Vente, Phys. Rev. B **54**, 15 967 (1996).
[22] R. Seshadri, A. Maignan, M. Hervieu, N. Nguyen, and B. Raveau, Solid State Commun. **101**, 453 (1997).
[23] T. Akimoto, Y. Moritomo, K. Ohoyama, S. Okamoto, S. Ishihara, S. Maekawa, K. Hirota, and A. Nakamura, Phys. Rev. B **61**, 11 270 (2000).
[24] C. D. Ling, J. E. Millburn, J. F. Mitchell, D. N. Argyriou, J. Linton, and H. N. Bordallo, Phys. Rev. B **62**, 15 096 (2000).
[25] L. M. Rodriguez-Martinez and J. P. Attfield, Phys. Rev. B **54**, R15 622 (1996).
[26] Y. Ohta, T. Tohyama, and S. Maekawa, Phys. Rev. B **43**, 2968 (1991).
[27] J. Zaanen, G. A. Sawatzky, and J. W. Allen, Phys. Rev. Lett. **55**, 418 (1985).
[28] T. Arima, Y. Tokura, and J. B. Torrance, Phys. Rev. B **48**, 17 006 (1993).
[29] P. K. de Boer and R. A. de Groot, Phys. Rev. B **60**, 10 758 (1999).
[30] S. Ishihara, S. Okamoto, and S. Maekawa, J. Phys. Soc. Jpn. **66**, 2965 (1997).
[31] J. C. Slater, in *Quantum Theory of Atomic Structure* (McGraw Hill, New York, 1960) Vol. 1.
[32] S. Ishihara, J. Inoue, and S. Maekawa, Physica C **263**, 130 (1996); Phys. Rev. B **55**, 8280 (1997).
[33] S. Okamoto, S. Ishihara, and S. Maekawa, Phys. Rev. B **61**, 451 (2000).
[34] S. Okamoto, S. Ishihara, and S. Maekawa, Phys. Rev. B **61**, 14 647 (2000); Y. Endoh, K. Hirota, S. Ishihara, S. Okamoto, Y. Murakami, A. Nishizawa, T. Fukuda, H. Kimura, H. Nojiri, K. Kaneko, and S. Maekawa, Phys. Rev. Lett. **82**, 4328 (1999).
[35] R. Maezono and N. Nagaosa, Phys. Rev. B **61**, 1825 (2000).
[36] S. Ishihara, M. Yamanaka, and N. Nagaosa, Phys. Rev. B **56**, 686 (1997).
[37] R. Maezono, S. Ishihara, and N. Nagaosa, Phys. Rev. B **57**, R13 993 (1998).